NASA CONTRACTOR REPORT

NASA CR-2783

DEVELOPMENT OF RELAXATION TURBULENCE MODELS

C. M. Hung

Prepared by
DCW INDUSTRIES
Sherman Oaks, Calif. 91423
for Ames Research Center

NATIONAL AERONAUTICS AND SPACE ADMINISTRATION · WASHINGTON, D. C. · DECEMBER 1976

1. Report No.	2. Government Accession No.	3. Recipient's Catalog No.
NASA CR-2783		

4. Title and Subtitle	5. Report Date
DEVELOPMENT OF RELAXATION TURBULENCE MODELS	December 1976
	6. Performing Organization Code

7. Author(s)	8. Performing Organization Report No.
C. M. Hung	
	10. Work Unit No.

9. Performing Organization Name and Address	11. Contract or Grant No.
DCW Industries 13535 Ventura Blvd., Suite 207 Sherman Oaks, California 91423	NAS 2-8995
	13. Type of Report and Period Covered
12. Sponsoring Agency Name and Address	Contractor Report
National Aeronautics and Space Administration Washington, D. C. 20546	14. Sponsoring Agency Code

15. Supplementary Notes

16. Abstract

Relaxation turbulence models have been intensively studied. The complete time-dependent mass-averaged Navier-Stokes equations have been solved for flow into a two-dimensional compression corner. The new numerical scheme developed by MacCormack has been incorporated into the developed computed code with an attendant order-of-magnitude reduction in computation time. The study consists of three interrelated parts. First, computed solutions are compared with experimental measurements of Law for supersonic flow for a Mach number, M_∞, of 2.96 and Reynolds number, Re_L, of 10^7, with wedge angle 25°. Details of the relaxation process have been studied; several different relaxation models, including different relaxation processes and varying relaxation length, are tested and compared. Then a parametric study has been conducted in which both Reynolds number and wedge angle are varied. To assess effects of Reynolds number and wedge angle, the parametric study includes the comparison of computed separation location and upstream extent of pressure rise; numerical results are also compared with the measurements of surface pressure, skin friction and mean velocity field for $M_\infty = 2.86$, $Re_{\delta_o} = 1.3\times10^6$ and $\alpha = 24°$, by Settle, Vas and Bogdonoff. Finally, the relaxation model is applied to hypersonic flow cases in which $M = 8.66$, $Re_L = 2.2\times10^7$ with a highly cooled wall and wedge angles $\alpha = 27°$ and 36°.

In general, the equilibrium model predicts a sharp increase in the outer-layer eddy viscosity near the separation shock; by contrast, the relaxation process substantially decreases the eddy viscosity and predicts better upstream pressure propagation. The simple eddy viscosity model predicts, with very good agreement, upstream boundary conditions even in the hypersonic flow with heat transfer. However, it under-predicts the eddy viscosity, and hence the skin friction, in the reattachment and downstream recompression regions. The relaxation process reduces the eddy viscosity further, and shows unfavorable effects on heat transfer, skin friction and reattachment points in these regions, thus indicating a need for further development and improvement of the relaxation concept.

17. Key Words (Suggested by Author(s))	18. Distribution Statement
Turbulent flow, Relaxation Model, Supersonic, Compression Corner	Unlimited STAR Category - 34

19. Security Classif. (of this report)	20. Security Classif. (of this page)	21. No. of Pages	22. Price*
Unclassified	Unclassified	38	$3.25

*For sale by the National Technical Information Service, Springfield, Virginia 22161

FOREWORD

This report presents results of an investigation of relaxation turbulence models. The work was done by personnel of DCW Industries for the Thermo- and Gas-Dynamics Division of the NASA Ames Research Center under Contract NAS2-8995. The technical monitors for the study were Mr. M. Inouye and Mr. R.W. MacCormack, Computational Fluid Dynamics Branch, NASA Ames Research Center, Moffett Field, California.

ABSTRACT

Relaxation turbulence models have been intensively studied. The complete time-dependent mass-averaged Navier-Stokes equations have been solved for flow into a two-dimensional compression corner. The new numerical scheme developed by MacCormack has been incorporated into the developed computed code with an attendant order-of-magnitude reduction in computation time. The study consists of three interrelated parts. First, computed solutions are compared with experimental measurements of Law for supersonic flow for a Mach number, M_∞, of 2.96 and Reynolds number, Re_L, of 10^7, with wedge angle 25°. Details of the relaxation process have been studied; several different relaxation models, including different relaxation processes and varying relaxation length, are tested and compared. Then a parametric study has been conducted in which both Reynolds number and wedge angle are varied. To assess effects of Reynolds number and wedge angle, the parametric study includes the comparison of computed separation location and upstream extent of pressure rise; numerical results are also compared with the measurements of surface pressure, skin friction and mean velocity field for $M_\infty = 2.86$, $Re_{\delta_o} = 1.3 \cdot 10^6$ and $\alpha = 24°$, by Settles, Vas and Bogdonoff. Finally, the relaxation model is applied to hypersonic flow cases in which $M_\infty = 8.66$, $Re_L = 2.2 \cdot 10^7$ with a highly cooled wall and wedge angles $\alpha = 27°$ and 36°.

In general, the equilibrium model predicts a sharp increase in the outer-layer eddy viscosity near the separation shock; by contrast, the relaxation process substantially decreases the eddy viscosity and predicts better upstream pressure propagation. The simple eddy viscosity model predicts, with very good agreement, upstream boundary conditions even in the hypersonic flow with heat transfer. However, it under-predicts the eddy viscosity, and hence the skin friction, in the reattachment

and downstream recompression regions. The relaxation process reduces the eddy viscosity further, and shows unfavorable effects on heat transfer, skin friction and reattachment points in these regions, thus indicating a need for further development and improvement of the relaxation concept.

CONTENTS

NOTATION

SYMBOL	DEFINITION
A	Damping length for sublayer eddy viscosity
C_p	Pressure coefficient, $2p_w/\rho_\infty u_\infty^2$
C_H	Heat transfer coefficient (Stanton number)
C_f	Skin friction coefficient, $2\tau_w/\rho_\infty u_\infty^2$
C_v	Specific heat at constant volume
D	Van Driest damping factor
E	Total energy, $\rho[e + 0.5(u^2 + v^2)]$
e	Specific internal energy, $C_v T$
$\vec{H}$	Vector fluxes in Reynolds mass-averaged Navier-Stokes equation
h	Vertical dimension of computational domain
h_f	Vertical dimension of fine mesh
K	Von Karman's constant, 0.4
L	Characteristic length between leading edge and wedge
L_o	Upstream boundary location
M_∞	Freestream Mach number
Pr	Molecular Prandtl number, 0.72
Pr_t	Turbulent Prandtl number, 0.90
p	Average static pressure, $p = \rho RT$
$\vec{Q}$	Heat flux vector, $Q_x\vec{e}_x + Q_y\vec{e}_y$
Q_x, Q_y	Heat flux components in Cartesian coordinates
$\vec{q}$	Velocity vector, $u\vec{e}_x + v\vec{e}_y$
Re_L	Reynolds number based on characteristic length L
T	Absolute temperature, °R

NOTATION (continued)

SYMBOL	DEFINITION
t	Time
U	Vector component of conserved properties in Equation (1)
u_e	Velocity at the edge of boundary layer
u_τ	Friction velocity, $u_\tau = \sqrt{\tau_w/\rho_w}$
u,v	Velocity components in Cartesian coordinates
x_o	Initial relaxation location, Equation (5)
x_w	Distance along the wall
x,y	Cartesian coordinates
Δx_p	Upstream pressure rise length
Δx_s	Separation length
y^+	Dimensionless y distance, $y^+ = \rho_w u_\tau y/\mu_w$
y_1^+	The y^+ of the first mesh point
α	Wedge angle
β	Intermittency correction factor
γ	Specific heat ratio, 1.4
δ	Local boundary-layer thickness
δ_o	Boundary-layer thickness at the initial location x_o
δ^*	Kinematic displacement thickness
ε	Turbulent dynamic eddy viscosity used in calculation
ε_{eq}	Local equilibrium eddy viscosity, Equation (4)
μ	Molecular viscosity
μ_w	Molecular viscosity at the wall
ρ	Mass-averaged specific density

NOTATION (concluded)

SYMBOL	DEFINITION
$\overleftrightarrow{\tau}$	Stress tensor, see Equation (1)
τ_w	Shear stress at the wall
λ	Relaxation length

1. INTRODUCTION

Development of turbulence models is a prime factor for flow-field simulation. For strong nonequilibrium turbulent flows, superiority of current one- or two-equation models over zero-equation models remains unproven;[1-3] more sophisticated models such as those based on the Reynolds-stress equations and sub-grid turbulence formulations require large (possibly impractical) computation times. Hence, development of a modified simple eddy viscosity model for nonequilibrium turbulent flow is a very attractive approach for solving the Navier-Stokes equations if the concept is at all feasible.

The idea of nonequilibrium turbulence was realized by Jacobs[4] in 1939 and also by Prandtl[5] in 1945. Prandtl[5] studied fully developed turbulence and pointed out that the state of turbulence at any given moment consists partly of a residual contribution from the previous flow history. Rotta[6] concluded from experimental data that when turbulent flow is perturbed from its equilibrium state, it takes a distance about one order of magnitude greater than its boundary layer thickness to attain a new equilibrium state. To account for this effect, Shang and Hankey[7] used an eddy viscosity relaxation model and solved the Navier-Stokes equations for a compression corner. Their results were sufficiently promising to encourage further research aimed at generalizing the simple eddy viscosity model to include previous turbulence history for nonequilibrium supersonic turbulent flows subjected to strong adverse pressure gradients.

In more recent applications, Baldwin and Rose,[8] and Shang, Hankey, and Law[9] also used the relaxation model to simulate shock impingement problems, and found results which were a significant improvement over those obtained with the simple

eddy viscosity model. Deiwert[10] extended the relaxation model to simulate a transonic flow over a thick airfoil, and Mateer, Brosh, and Viegas[11] used a similar model to calculate a transonic normal shock-wave boundary-layer interaction. Even though the latter results qualitatively represent the interactive features, Mateer, Brosh, and Viegas[11] indicated some unfavorable effects on skin friction attending use of the relaxation model.

The objectives of this study are: to understand how the relaxation model works; to study several different relaxation processes; and to examine the applicability of the model for high Mach number flows with heat transfer. The end result will hopefully provide some information for further turbulence model development.

2. ANALYSIS

2.1 GOVERNING EQUATIONS

The viscous-inviscid interaction flowfield is governed by the time-dependent, compressible Navier-Stokes equations. Casting in terms of Reynolds mass-averaged variables, and with the bulk viscosity and the specific turbulent energy in the normal stress components omitted, the resulting mean conservative relations are the same as their laminar flow counterpart, except for the addition of the Reynolds stress tensor and the Reynolds heat flux. Turbulent closure is accomplished by expressing the Reynolds stress tensor in terms of the product of eddy viscosity ε with the mean velocity gradients. Also, a turbulent Prandtl number, Pr_t, is used for the Reynolds heat flux. Thus, the mean flow equations in two dimensions can be written in integral form as

$$\frac{\partial}{\partial t}\int_{volume} U \, dVol + \int_{surface} \vec{H} \cdot \vec{n} \, dS = 0 \qquad (1)$$

where

$$U = \begin{pmatrix} \rho \\ \rho u \\ \rho v \\ E \end{pmatrix} \qquad \vec{H} = \begin{pmatrix} \rho\vec{q} \\ \rho u\vec{q} + \vec{\vec{\tau}} \cdot \vec{e}_x \\ \rho v\vec{q} + \vec{\vec{\tau}} \cdot \vec{e}_y \\ E\vec{q} + \vec{\vec{\tau}} \cdot \vec{q} + \vec{Q} \end{pmatrix}$$

$$\vec{q} = u\vec{e}_x + v\vec{e}_y$$

$$\vec{\vec{\tau}} = \sigma_x \vec{e}_x\vec{e}_x + \tau_{xy}\vec{e}_x\vec{e}_y + \tau_{yx}\vec{e}_y\vec{e}_x + \sigma_y\vec{e}_y\vec{e}_y$$

$$\sigma_x = p + \frac{2}{3}(\mu+\varepsilon)\left(\frac{\partial u}{\partial x} + \frac{\partial v}{\partial y}\right) - 2(\mu+\varepsilon)\frac{\partial u}{\partial x}$$

$$\tau_{xy} = \tau_{yx} = -(\mu+\varepsilon)\left(\frac{\partial u}{\partial y} + \frac{\partial v}{\partial x}\right)$$

$$\sigma_y = p + \frac{2}{3}(\mu+\varepsilon)\left(\frac{\partial u}{\partial x} + \frac{\partial v}{\partial y}\right) - 2(\mu+\varepsilon)\frac{\partial v}{\partial y}$$

$$\vec{Q} = Q_x\vec{e}_x + Q_y\vec{e}_y$$

$$Q_x = -\left(\frac{\mu}{Pr} + \frac{\varepsilon}{Pr_t}\right)\gamma\frac{\partial e}{\partial x}$$

$$Q_y = -\left(\frac{\mu}{Pr} + \frac{\varepsilon}{Pr_t}\right)\gamma\frac{\partial e}{\partial y}$$

$$E = \rho\left[e + 0.5(u^2 + v^2)\right]$$

and $\vec{e}_x$, $\vec{e}_y$ are unit vectors of the orthogonal (x,y) coordinate system, and $\vec{n}$ a unit normal vector of the surface enclosing the volume of integration. The equation of state relates the pressure, p, and density, ρ, to temperature, T, and specific internal energy, e. The perfect gas relations are

$$p = \rho RT \quad \text{and} \quad e = C_v T$$

The molecular viscosity coefficient, μ, is assumed to be a function of temperature only, and is evaluated by Sutherland's semi-empirical formula

$$\mu = 2.270\cdot10^{-8}\ T^{3/2}/(T + 198.6) \quad \text{(slug/ft·sec)}$$

In the present calculation, molecular Prandtl number, Pr, is assumed to be 0.72 and turbulent Prandtl number, Pr_t, is taken to be 0.90.

2.2 COMPUTATIONAL DOMAIN

Figure 1 shows the computational domain and appropriate boundary conditions. The mesh is equally spaced in the x-direction. In the y-direction, a fine, geometrically-stretched mesh spacing is used in the region near the wall ($y \leq h_f$) for resolving the viscous layer; a coarse, equally-spaced mesh is used in the outer region ($h_f < y < h$), where viscous effects are negligible.

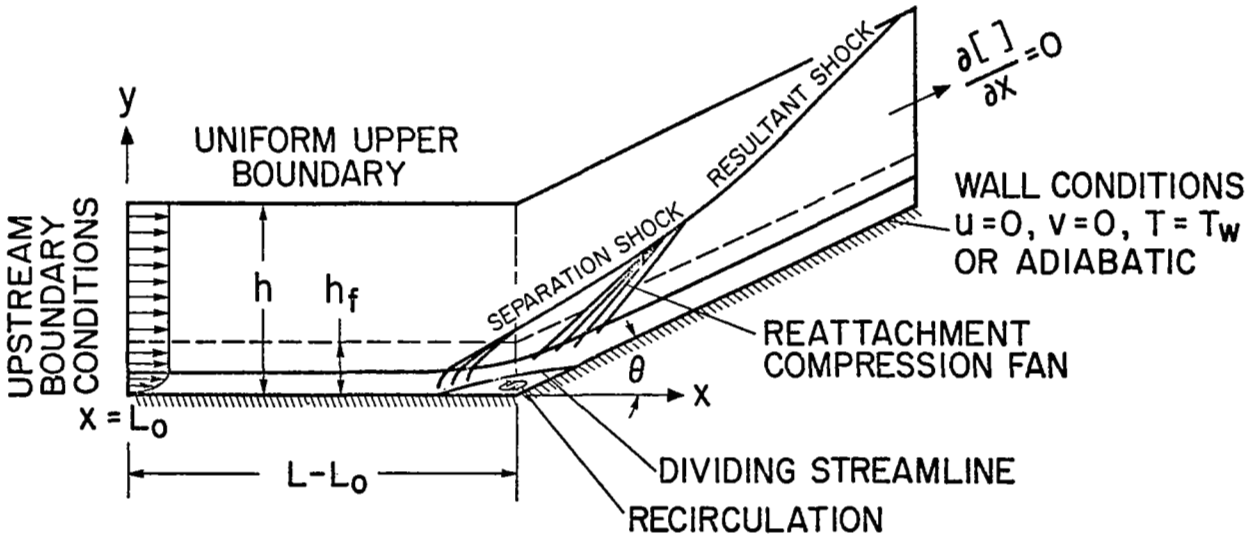

Figure 1. Computational domain and boundary conditions.

The upstream boundary is located at a distance several boundary-layer thicknesses ahead of the interaction region defined from when the pressure starts to increase until it reaches its final value. The upstream conditions can be either generated from the present program by solving the Navier-Stokes equations over a flat plate that includes leading edge effects, or supplied from a conventional boundary-layer solution, such as Marvin and Sheaffer's boundary-layer code.[12] The downstream boundary is positioned far enough from the corner so that all the gradients in the flow direction can be set to zero. Though this condition is not exact, the boundary layer in the vicinity of this exit is parabolic, and the remainder of the flow is supersonic; hence, this condition is not expected to introduce significant error in the region of interest upstream. The upper boundary is specified by the freestream conditions. The wall surface is assumed impermeable, and no-slip boundary conditions are applied. The wall is treated either as isothermal or adiabatic, and the wall pressure is evaluated from an approximation of the y-momentum equation at the wall. During the calculation on the inner mesh, transport and stress at the internal boundary, $y = h_f$, are saved, and their net quantities are then used as boundary conditions for the outer mesh flowfield.

The numerical method and special numerical procedures used in the calculation presented herein are described in detail in References 13 and 14. The computer code was initially checked out for laminar flow cases to ensure that the numerical scheme is accurate and efficient. (Details of laminar flow results are presented in Reference 14.) The same code is used herein to test the adequacy of turbulence models. During the course of the study the new numerical method developed by MacCormack[15] was incorporated in the computer code. This new method reduced computer times by an order of magnitude, thus facilitating economically feasible parametric studies (c.f., Subsection 3.5).

2.3 EDDY VISCOSITY MODEL

In the present study, a two-layer equilibrium eddy viscosity model ("equilibrium model") is applied in the following fashion: In the inner region, the Prandtl mixing-length concept is used

$$\varepsilon_{inner} = \rho(KyD)^2\left[\left(\frac{\partial u}{\partial y}\right)^2 + \left(\frac{\partial v}{\partial x}\right)^2\right]^{\frac{1}{2}} \tag{2}$$

where K is the von Karman's constant (0.4) and D is van Driest's damping factor

$$D = 1 - \exp(-y/A) \quad , \quad A = 26\,\mu/\left(\sqrt{|\tau_w|\rho}\right)$$

In the law of the wall for the outer region, the modified Clauser's defect law is employed

$$\varepsilon_{outer} = 0.0168\ \rho u_e \delta^* \beta \tag{3}$$

where β is the Klebanoff intermittency correction factor

$$\beta = \left[1 + 5.5(y/\delta)^6\right]^{-1}$$

and

$$u_e = u \quad \text{at } y = \delta \text{ (edge of boundary layer)}$$

$$\delta^* = \int_{y_o}^{\delta}\left(1 - \frac{u}{u_e}\right)dy$$

$$\delta = \text{minimum of } (\delta_1,\delta_2), \quad \begin{cases} \delta_1 = y\,|\,[\max(\rho u),\ J < J_{max}] \\ \delta_2 = u\,|\,[(\Delta u/u) < 0.02] \end{cases}$$

The quantity y_o is the location of zero velocity and J_{max} is a preassigned value, ensuring it is located outside the boundary layer. Then the eddy viscosity is determined by

$$\varepsilon_{eq} = \begin{cases} \varepsilon_{inner} & \text{if } y < y_i \\ \varepsilon_{outer} & \text{if } y > y_i \end{cases} \qquad (4)$$

where y_i is the first point that $\varepsilon_{outer} < \varepsilon_{inner}$. A simple smoothing is also applied on A and δ^*.

Note that the local values of μ and ρ are used in A, as opposed to the more conventional format of using the wall values, a difference which might become significant in highly cooled or heated wall calculations. Use of y_o as the lower bound for the integration of δ^* avoids picking up the unwanted negative (reverse) flow effects in evaluating the displacement thickness. The main difference of the presently employed equilibrium model from that used by Shang and Hankey[7] is that the velocity at the edge of boundary layer u_e (instead of the maximum velocity u_{max}) is used in the calculation of outer-layer eddy viscosity, ε_{outer}, and the displacement thickness, δ^*. Although it is difficult in viscous-inviscid interactions to determine the edge of the boundary layer, care should be taken to determine u_e. Without this effort, the maximum velocity, in general, will be the freestream velocity, instead of the more typical boundary-layer edge velocity behind the induced shock. Use of the freestream velocity will overestimate δ^*, and, in our experience, may cause up to a factor of two-or-more difference in the calculation of outer-layer eddy viscosity, ε_{outer}.

3. COMPARISON AND DISCUSSION OF RESULTS

3.1 SUPERSONIC FLOW APPLICATIONS

The first case computed was for $M_\infty = 2.96$ supersonic flow over a 25° wedge with an adiabatic wall. The flow conditions correspond identically with one of the cases studied by Shang and Hankey[7] and with experimental data measured by Law.[16] Flow conditions are as follows:

$M_\infty = 2.96$ $\quad Re_L = 10^7$ $\quad \alpha = 25°$

$T_\infty = 177°R$ $\quad L = 1$ ft $\quad$ adiabatic wall

The computational domain extends from $x/L = 0.795$ to $x/L = 1.205$ with the fine mesh boundary placed at $h_f = 0.025$ ft and the outer boundary at $h = 0.09$ ft. In the x-direction 63 mesh points are used; in the y-direction, a total of 31 mesh points, 20 for the fine mesh and 11 for the coarse mesh, are used. The mesh spacing varies from $(\Delta y)_{min} = 0.148 \cdot 10^{-3}$ ft to $\Delta y = 0.446 \cdot 10^{-2}$ ft for the fine mesh, and near the wall the mesh cells are very elongated with a ratio of $\Delta x : (\Delta y)_{min} = 44:1$. For the case of interest, the compression is moderate (the pressure rise is about a factor of 5); the boundary-layer thickness is about the same before and after the interaction. Therefore, $(\Delta y)_{min}$ is fine enough to ensure that the first mesh points near the wall are in the sublayer ($y_1^+ < 10$) both upstream and downstream of the compression.

The upstream conditions are generated with the present numerical code by solving the flow over a flat plate with a leading edge. Figure 2 shows a u-velocity profile compared with a boundary-layer solution[12] and Shang and Hankey's result.[7] The agreement is very good. Plotted on the nondimensional scale of (u/u_τ) vs y^+, the profile is in surprisingly good agreement with the law of the wall (Figure 3). The value of y^+ of the first mesh point of the present study is about 5.8 and that of

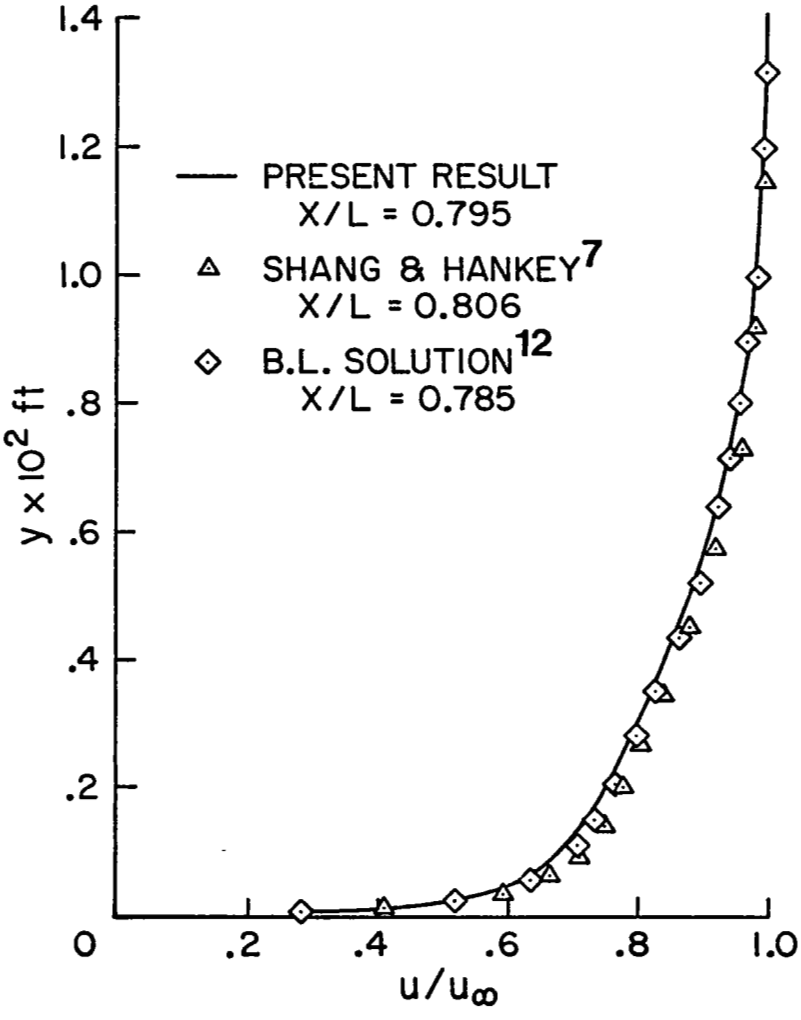

Figure 2. Flat-plate solution; $M_\infty = 2.96$, $Re_L = 10^7$.

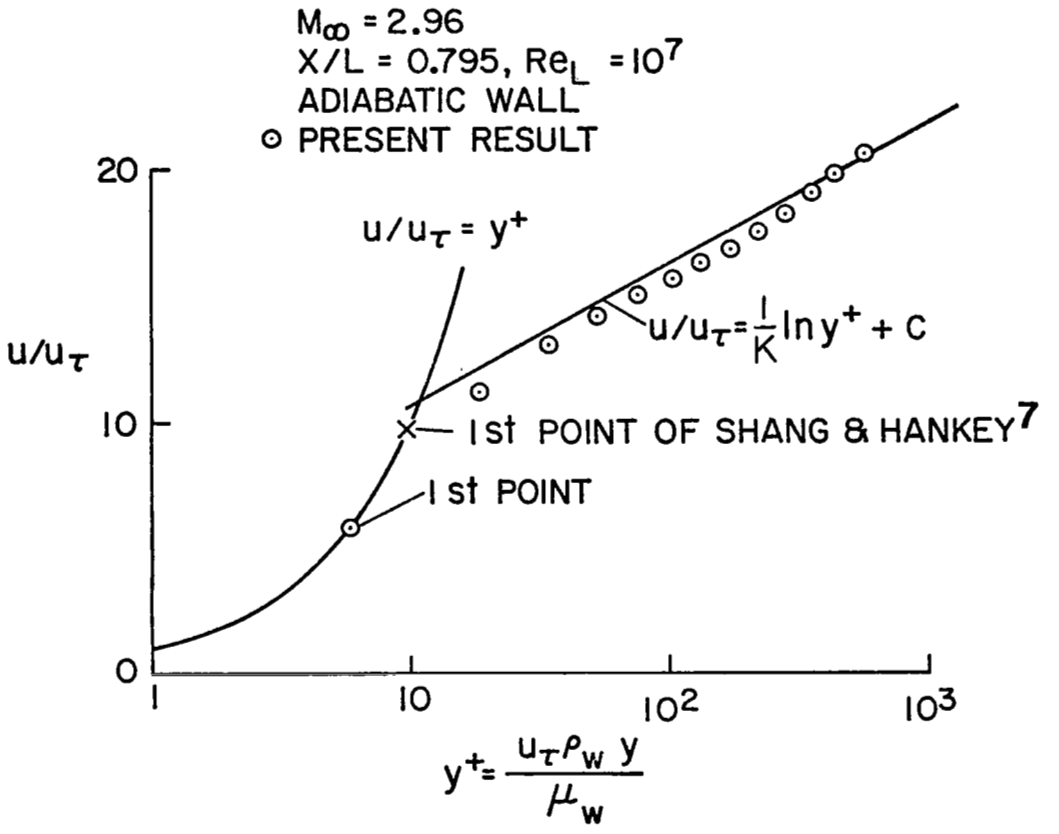

Figure 3. Law of the wall.

Reference 7 is just under 10. Figures 4(a) and 4(b) show comparisons of pressure and skin friction calculated using the present equilibrium model with the experimental measurements of Law.[16] The equilibrium model tends to overpredict the surface pressure in the reattachment and downstream regions, and underpredicts the upstream pressure rise and, thus, the location of the separation point. Also shown in these two figures is a comparison of the equilibrium results of Reference 7 with those of the present study. Even with the good agreement found upstream (Figure 2), the results here are substantially different because of the difference in formulating the eddy viscosity models. The use of u_{max}, instead of u_e, in Reference 7 tends to provide a higher eddy viscosity and thus more mixing inside the boundary layer, which makes it more resistant to separation. The modeling difference is relatively insensitive in the flat-plate solution, even though the boundary-layer profile in Reference 7 does show slightly more momentum from the increased mixing. In the interaction region where a shock wave lies above the boundary layer, it causes a significant difference.

3.2 UPSTREAM RELAXATION CONCEPT

To account for the upstream turbulence history effects, Shang and Hankey[7] used a relaxation eddy viscosity model (herein designated "upstream relaxation" or "relaxation"), i.e.,

$$\varepsilon = \varepsilon_{eq} - (\varepsilon_{eq} - \varepsilon_o) \exp\left(-\frac{x - x_o}{\lambda}\right) \tag{5}$$

where

ε = turbulence dynamic eddy viscosity

ε_{eq} = the local equilibrium eddy viscosity evaluated from Equation (4)

ε_o = the eddy viscosity at upstream location x_o

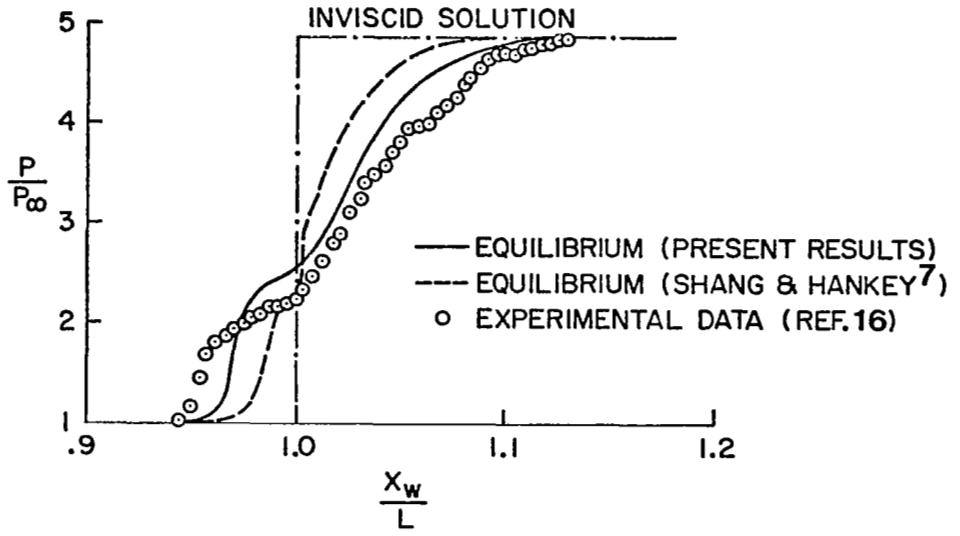

(a) Surface pressure.

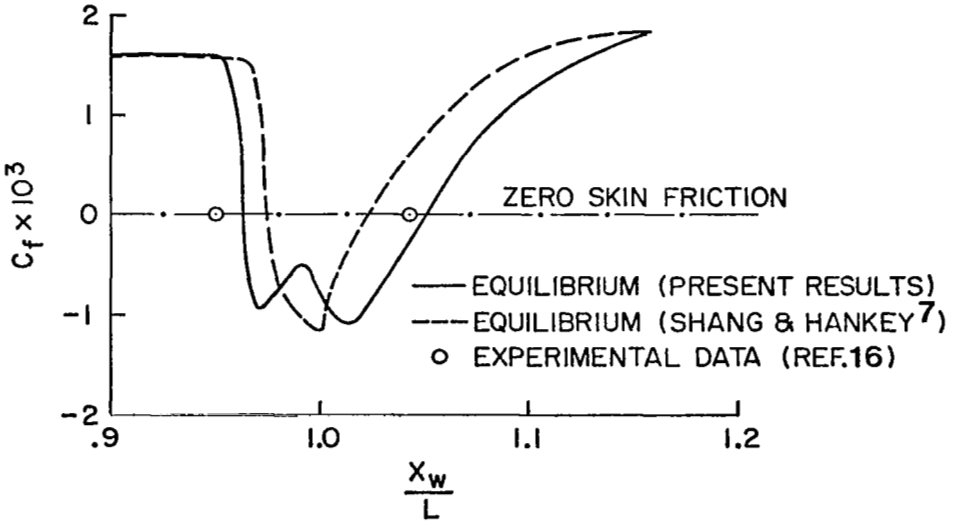

(b) Skin friction.

Figure 4. Comparison of the results of equilibrium models; $M_\infty = 2.96$, $\alpha = 25°$, $Re_L = 10^7$.

and λ is the relaxation length. Conceptually Equation (5) approximates the experimental observation that, in an abrupt disturbance of a turbulent flow, the Reynolds stress remains nearly frozen at its initial value while it is being convected along streamlines, and then exponentially approaches a new equilibrium state. In a numerical calculation, the initial location of disturbance from which the relaxation process is initiated, x_o, and a relaxation length scale which describes the exponential decay of the eddy viscosity distribution, λ, must be specified. There are two limiting cases which bound the relaxation length. For $\lambda = 0$, the turbulent eddy viscosity equals the local equilibrium value, and for $\lambda = \infty$, the initial value ε_o is frozen and is used everywhere in the region $x > x_o$.

Using the upstream relaxation model, good improvement in predictions of upstream pressure rise is obtained and a more pronounced pressure plateau region is clearly demonstrated [Figures 5(a) and 5(b)]. For the present supersonic case, the relaxation length is chosen to be $\lambda = 5\delta_o$, and the initial location is positioned at $x_o/L = 0.9387$. The figures also show the results of equilibrium and frozen cases, which bounds the effect of changing the relaxation length scale from $\lambda = 0$ to $\lambda = \infty$. In Figure 6, the calculated density contours, obtained by using the relaxation model, are compared with the interferogram and a schematic of the experimental flowfield in Reference 17. Details of the interaction pattern, including separation shock, separation, and reattachment shock are accurately simulated.

3.3 EXPLANATION OF HOW THE RELAXATION MODEL WORKS

Since the inclusion of relaxation effects results in improved comparisons of theory with experiment, it is important to understand how the relaxation model works. Figure 7 shows the variation of eddy viscosity at five levels from the wall,

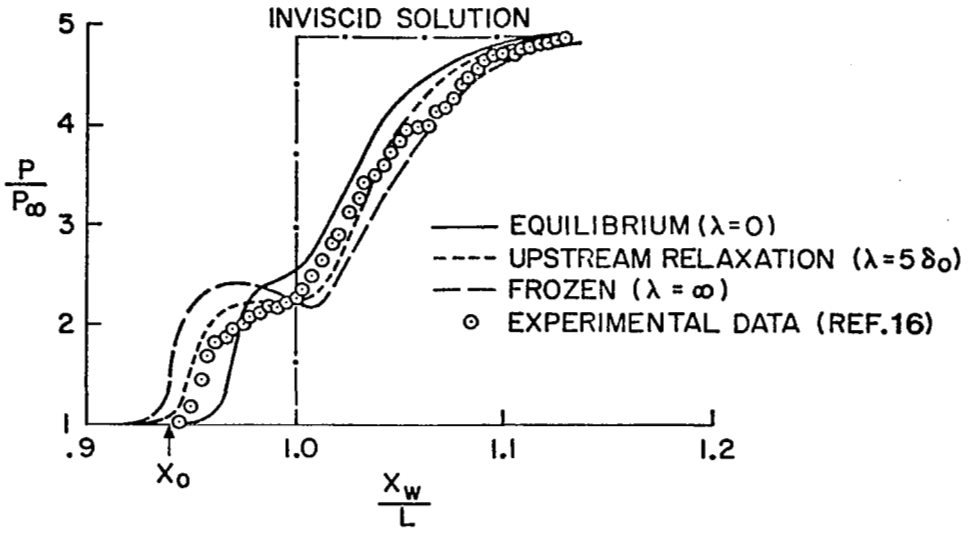

(a) Surface pressure.

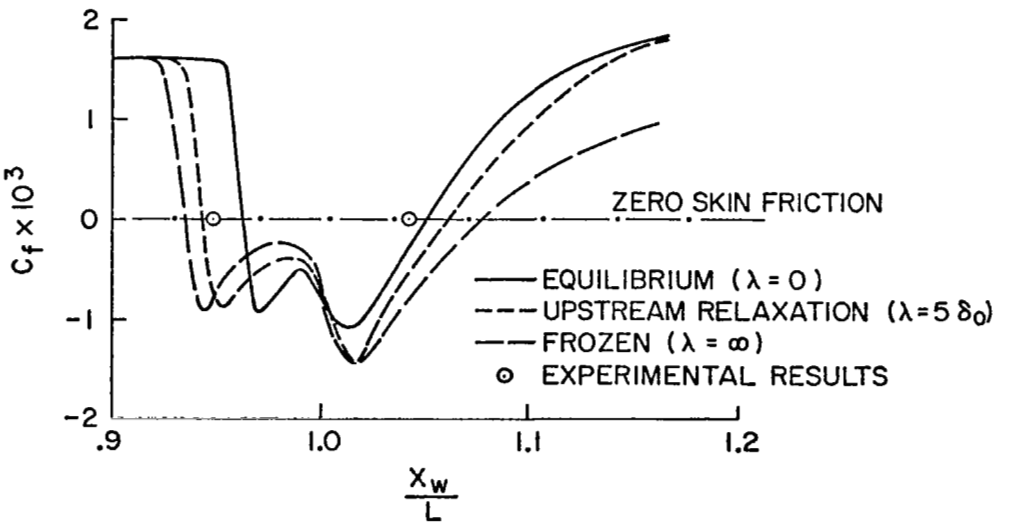

(b) Skin friction.

Figure 5. Results of different relaxation lengths; $M_\infty = 2.96$, $\alpha = 25°$, $Re_L = 10^7$, $\delta_o = 0.01403$ ft, $x_o/L = 0.9387$.

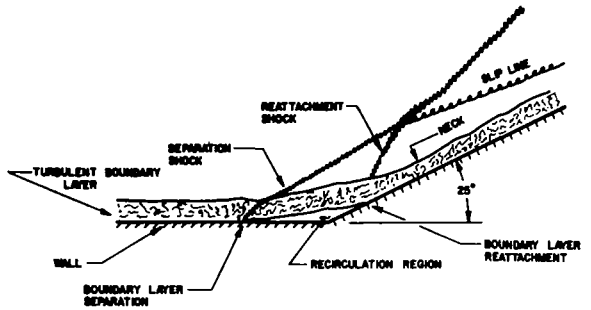

SCHEMATIC DIAGRAM OF FLOW FIELD

SUPERSONIC TURBULENT BOUNDARY LAYER OVER A COMPRESSION CORNER

($M_\infty = 2.96$, $R_{e_L} = 10^7$, $\alpha = 25°$)

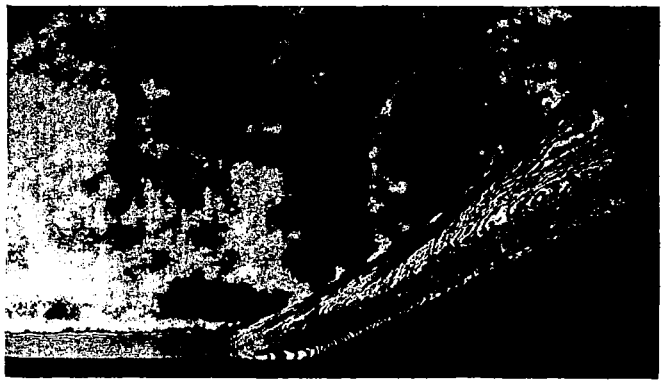

INTERFEROGRAM

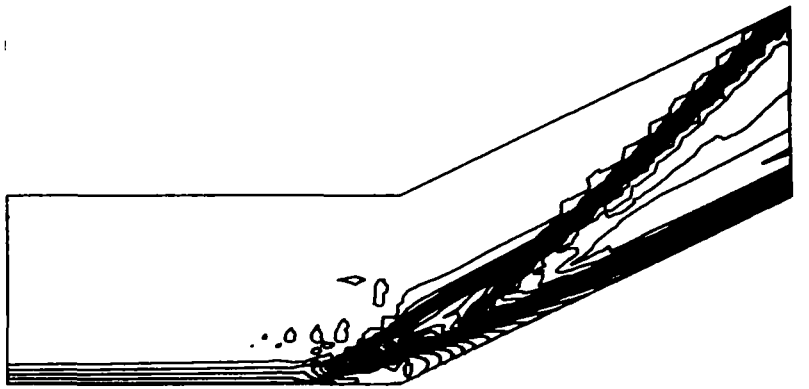

NUMERICAL SIMULATION (DENSITY CONTOURS)

Figure 6. Comparison of density contours with experimental intererogram; $M_\infty = 2.96$, $Re_L = 10^7$, $\alpha = 25°$.

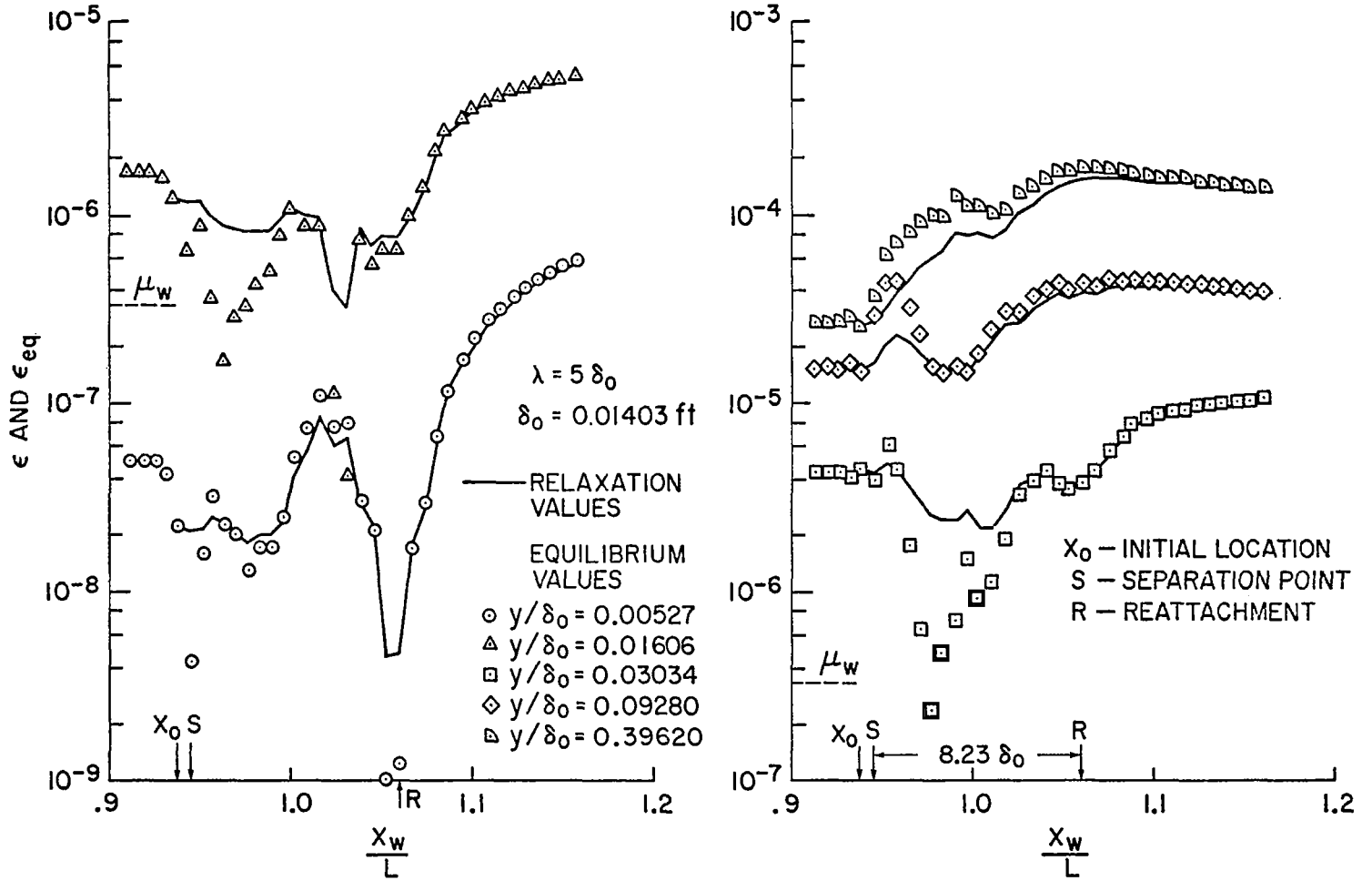

Figure 7. Eddy viscosity at five y-levels with upstream relaxation.

with the relaxation length $\lambda = 5\delta_o$. The symbols represent the values evaluated from the local equilibrium model, ε_{eq}, and the lines are the turbulent dynamic eddy viscosity which is based on the upstream relaxation formula, Equation (5). The first three sets of data (lines and symbols) for the smaller values of y belong to the inner layer of the eddy viscosity model; the data for $y/\delta_o = 0.0928$ are taken near the location of the transition from the inner to outer layers; and the outermost y-level data are calculated from the outer layer formula, Equation (3). Near the wall (circle symbols, Figure 7) the eddy viscosity is small, $\varepsilon_{eq} < \mu_w$, and is greatly dominated by the wall shear stress and the local velocity gradient [see Equation (2)]. At the beginning of the interaction, ε_{eq} near the wall decreases sharply because of the decrease of τ_w, reaching a minimum at separation. The minimum value of ε_{eq} appears again at the point of reattachment.

Note that $\tau_w = 0$ at the separation and reattachment points, and thus, from Equation (2), $D = 0$ and $\varepsilon_{inner} = 0$. Therefore, based on the local equilibrium model, [Equations (2)-(4)], there is no eddy viscosity, while in the real flow, turbulence fluctuations do exist at separation and reattachment. The application of the upstream relaxation process greatly increases the eddy viscosity values in these regions and only slightly affects the values in the downstream region when x/L is large.

In contrast to the effect at small y, ε_{eq} increases sharply at large y because of the increase in $\rho\delta^*$ resulting from the compression of the separation shock. The relaxation process drastically modifies the increasing slope and provides values of ε substantially less than that of the equilibrium model. The effects of the relaxation process can be examined more clearly in Figure 8, in which eddy viscosity profiles at three x-locations are plotted across the boundary layer. The reduction of eddy viscosity from its local equilibrium value far

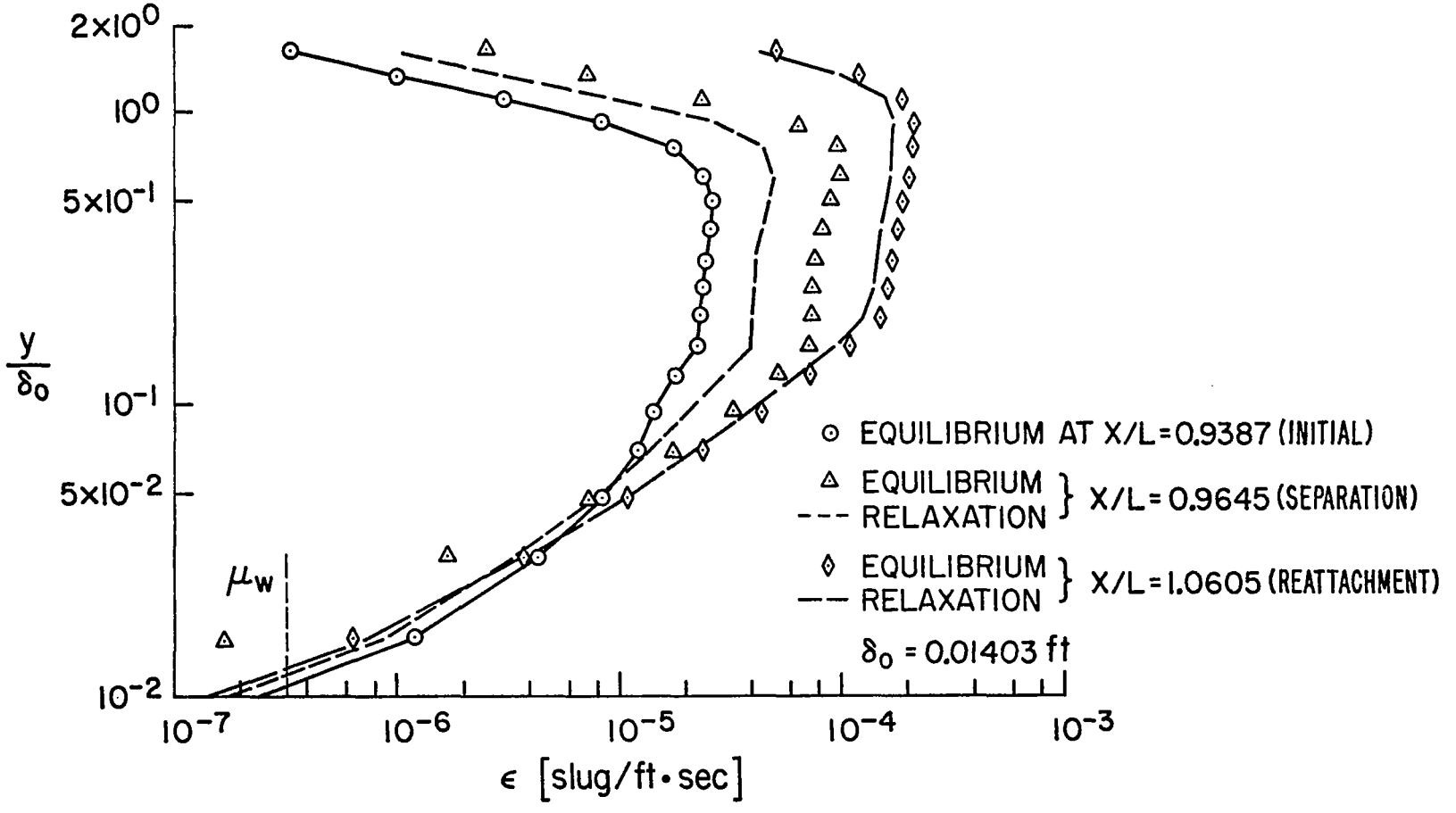

Figure 8. Eddy viscosity at three x locations.

from the wall leads to less turbulence mixing and to less shear stress to balance the adverse pressure gradient, making the separation easier, and allowing better upstream pressure rise through the viscous and inviscid interaction.

It is interesting to recall the result of the frozen case ($\lambda = \infty$) in which the initial value ε_o is used everywhere downstream of $x > x_o$. This causes the eddy viscosity in the outer region to be reduced by a factor of about 6 and, near the wall, by a factor of about 10, below the equilibrium value in the downstream region (see Figure 7 curves of $y/\delta_o = 0.00527$ and $y/\delta_o = 0.3962$). Hence, while the surface pressure closely reaches the value of the inviscid solution, the skin friction is a factor of about 2 less than the equilibrium result (see Figure 5b).

3.4 OTHER RELAXATION PROCESSES

In addition to the upstream relaxation model, other ways of controlling eddy viscosity were tried. One approach is based on the notion that the lagging phenomena is local point-by-point and should be governed by the following differential equation

$$\frac{d\varepsilon}{dx} = \frac{\varepsilon_{eq} - \varepsilon}{\lambda} \tag{6}$$

Equation (6) is closely approximated by the following formula[10,11] (herein called "point-by-point relaxation")

$$\varepsilon^i = \varepsilon^i_{eq} - \left(\varepsilon^i_{eq} - \varepsilon^{i-1}\right) \exp\left(\frac{x_i - x_{i-1}}{\lambda}\right)$$

This relaxation process avoids the question of specification of the upstream initial location x_o, instantly accounts for local upstream history while the turbulence conveys downstream, and can handle complex cases such as multiple shock disturbances, etc.

Another observation is that a great portion of the increase of dynamic eddy viscosity is caused by the increase of local density through shock compression. To separate the effect of the increase of density from the conveyance of turbulence history, the kinematic eddy viscosity is relaxed according to the upstream relaxation formula

$$\left(\frac{\varepsilon}{\rho}\right) = \left(\frac{\varepsilon}{\rho}\right)_{eq} - \left[\left(\frac{\varepsilon}{\rho}\right)_{eq} - \left(\frac{\varepsilon}{\rho}\right)_{o}\right] \exp\left(\frac{x - x_o}{\lambda}\right) \qquad (7)$$

Figures 9(a) and 9(b) compare results of these two different processes with the previous upstream relaxation result for surface pressure and skin friction. The point-by-point relaxation reduces the value of equilibrium eddy viscosity more, and results in a larger separation region. The relaxation of kinematic eddy viscosity [Equation (7)] has the opposite effect and is in very close agreement with the result of upstream relaxation in the downstream region where the relaxation effects are small.

The process of relaxing only the outer layer [Equation (3)] has also been tested. From experimental observation, it has been shown that the inner layer of a boundary layer subjected to any disturbance adjusts quickly back to local equilibrium, while the outer layer may take a much longer distance to return to a new state of equilibrium. The process of relaxing only the outer layer is an extreme case of varying the relaxing length across the boundary layer. It was found, however, that the result from relaxing only the outer layer agrees very closely with that from relaxing the whole boundary layer.

3.5 PARAMETRIC STUDY AND DETAIL COMPARISON

Instead of comparing the experimental surface pressure data of Law for six different wedge angles, the calculations were compared with newly available and more detailed data by

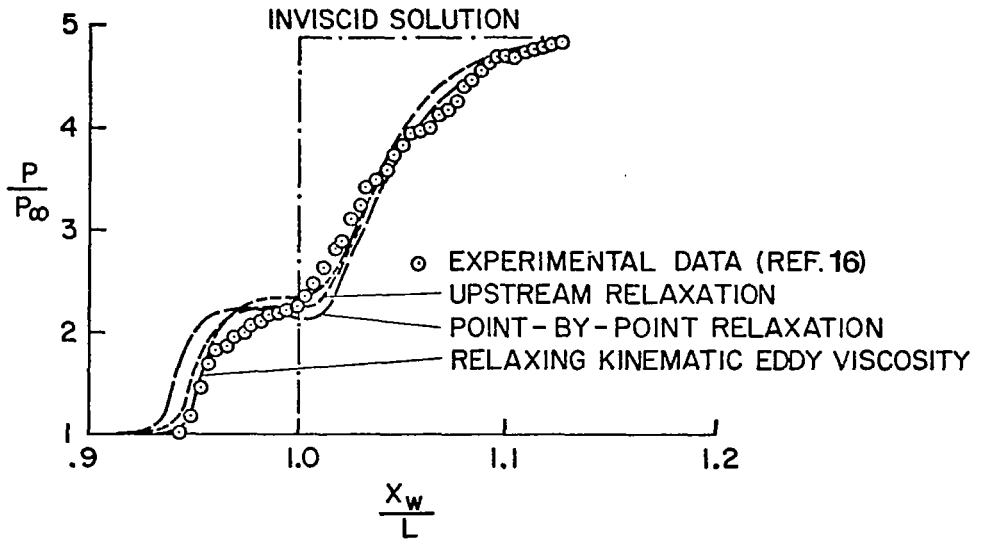

(a) Surface pressure.

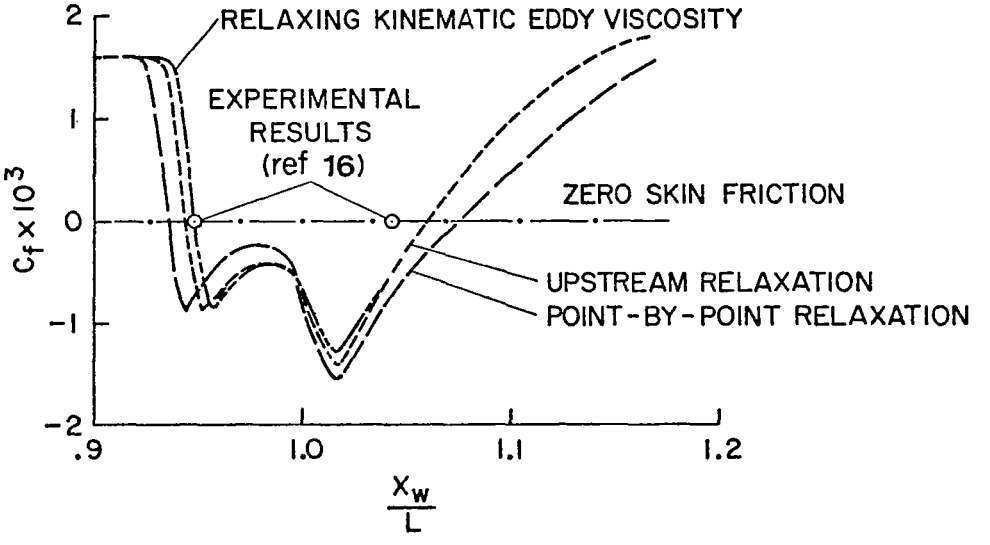

(b) Skin friction.

Figure 9. Results of different relaxation processes.

Settles, Vas and Bogdonoff.[18] The experiments were well-documented, including the measurements of surface pressure, skin friction and detailed mean velocity field, for a wide range of Reynolds numbers and shock strengths. Over 50 solutions have been obtained for the entire flowfield varying both Reynolds number and wedge angle. The results of these solutions are compared with corresponding experimental data in Figures 10-13. Figures 10(a) and 10(b) compare the separation locations while Figures 11(a) and 11(b) illustrate the upstream extent of the increased pressure level. Referring to the separation location comparisons, Figure 10(a) shows that for a wedge angle of 20° there is excellent agreement between the calculated values (with the equilibrium model) and experiment over the entire Reynolds number range. For the lower wedge angles the calculations show a larger separation distance than experiment. A crossplot of data at $Re_{\delta_o} = 1.33 \cdot 10^6$ [Figure 10(b)] shows that the calculated separation distance varies smoothly with wedge angle while the experimental data show an abrupt change near $\alpha = 16°$. The calculated upstream extent of the increased pressure level is compared with experiment in Figures 11(a) and 11(b). As shown, predicted trends with Reynolds number agree with measurements for either model. However, only the relaxation model predicts the correct magnitude.

Figures 12(a) and 12(b) compare predicted and measured surface pressure and skin friction for the $M_\infty = 2.85$, $Re_{\delta_o} = 1.3 \cdot 10^6$ and $\alpha = 24°$ case. The numerical results employ the three above-mentioned turbulence models and a fourth model combining the two modifications. Details of the "pressure gradient" model are discussed in Reference 19. Comparing the skin-friction distributions [Figure 12(b)], both the equilibrium and relaxation models substantially underpredict the skin friction downstream of reattachment. The calculated reattachment locations are also incorrect. While the calculations employing the

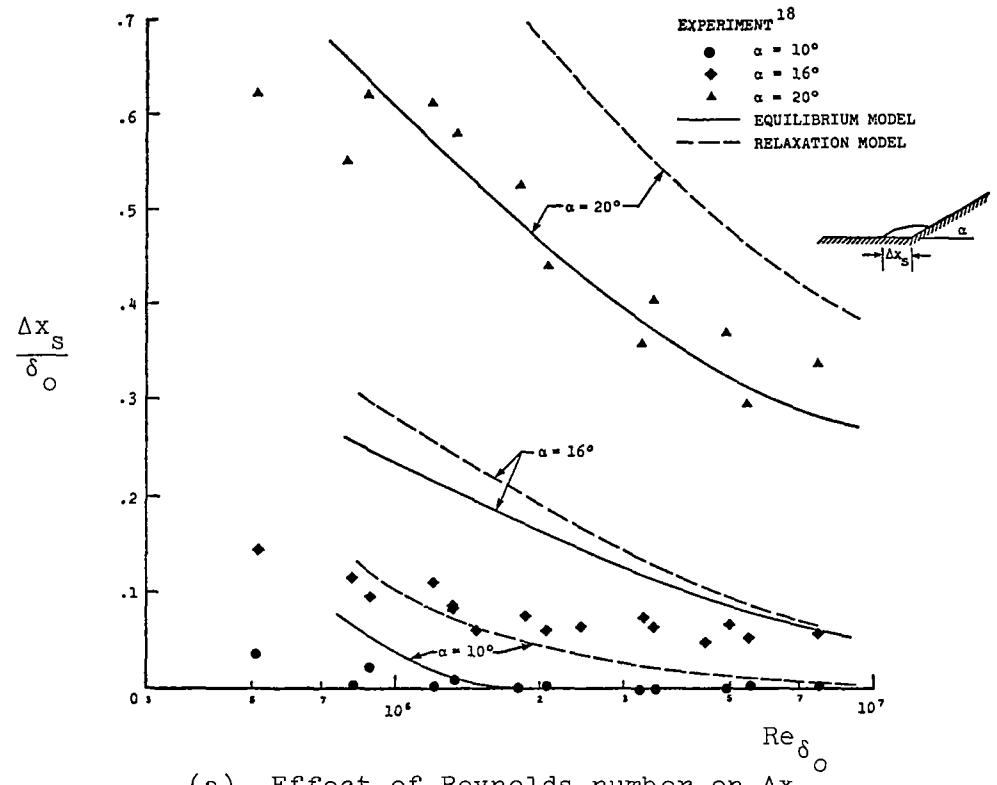

(a) Effect of Reynolds number on Δx_s.

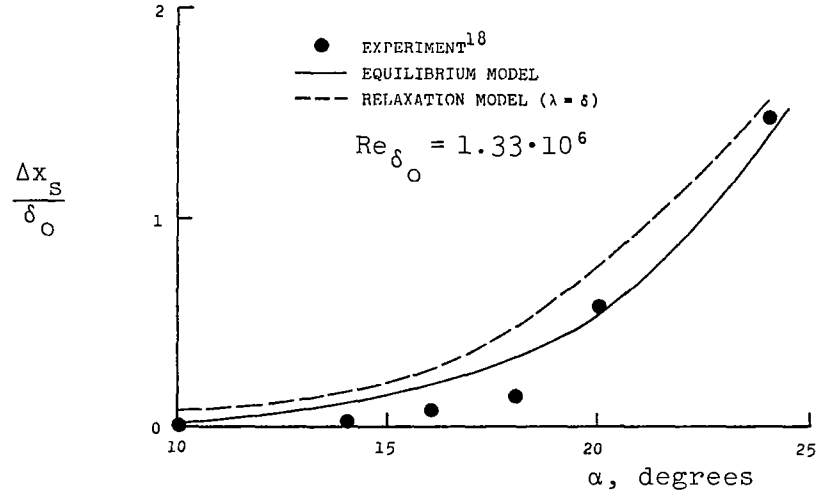

(b) Effect of wedge angle on Δx_s.

Figure 10. Comparison of computed and measured separation length, Δx_s.

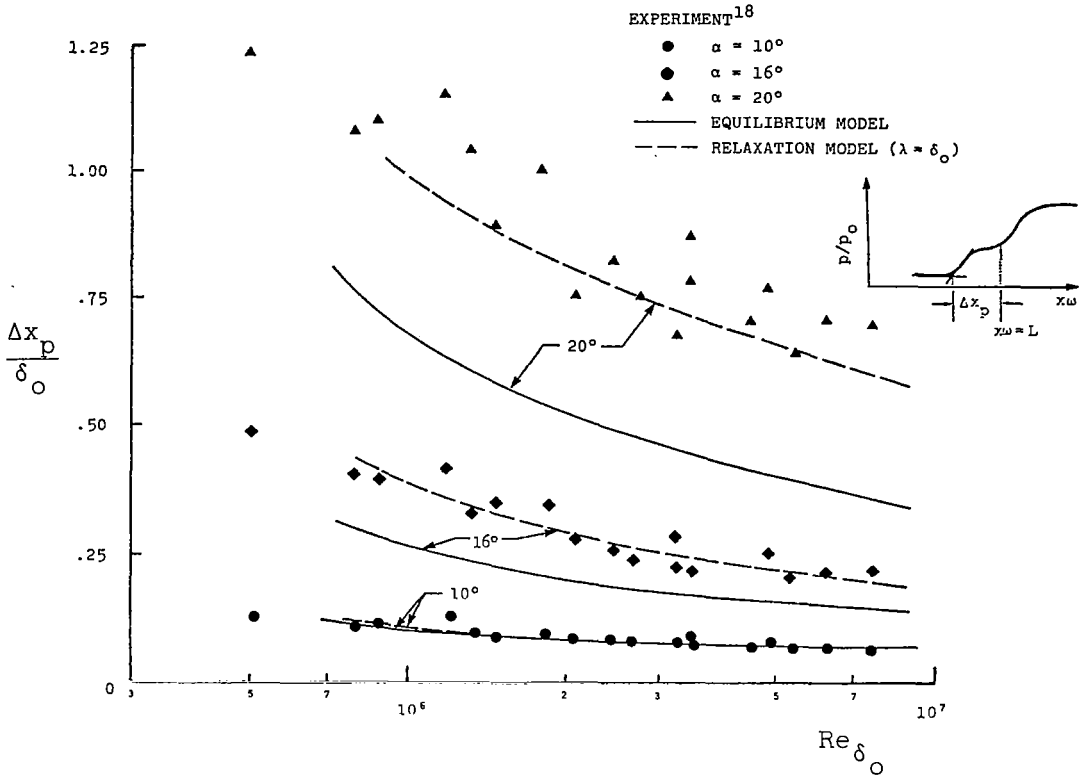

(a) Effect of Reynolds number on Δx_p.

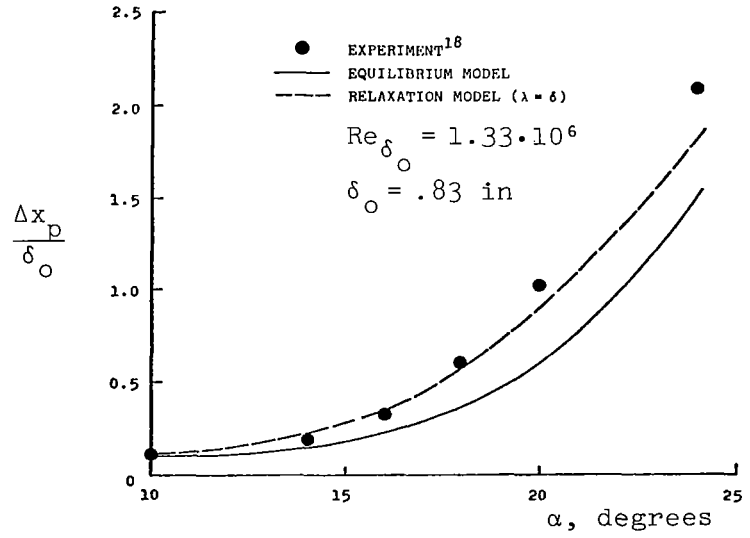

(b) Effect of wedge angle on Δx_p.

Figure 11. Comparison of computed and measured upstream pressure rise length, Δx_p; $M_\infty = 2.85$.

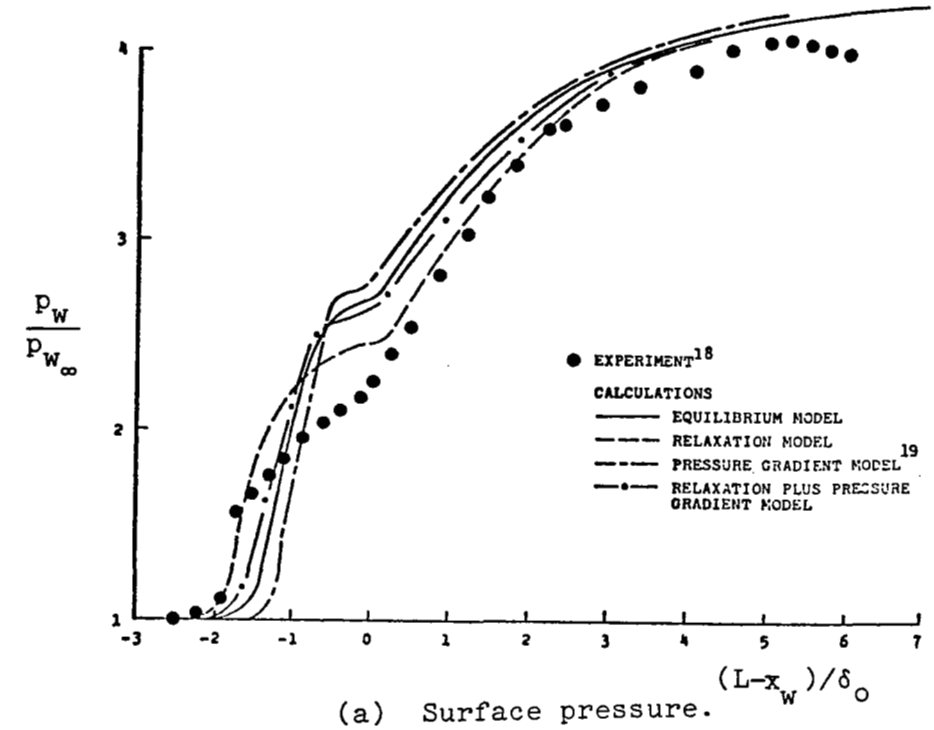

(a) Surface pressure.

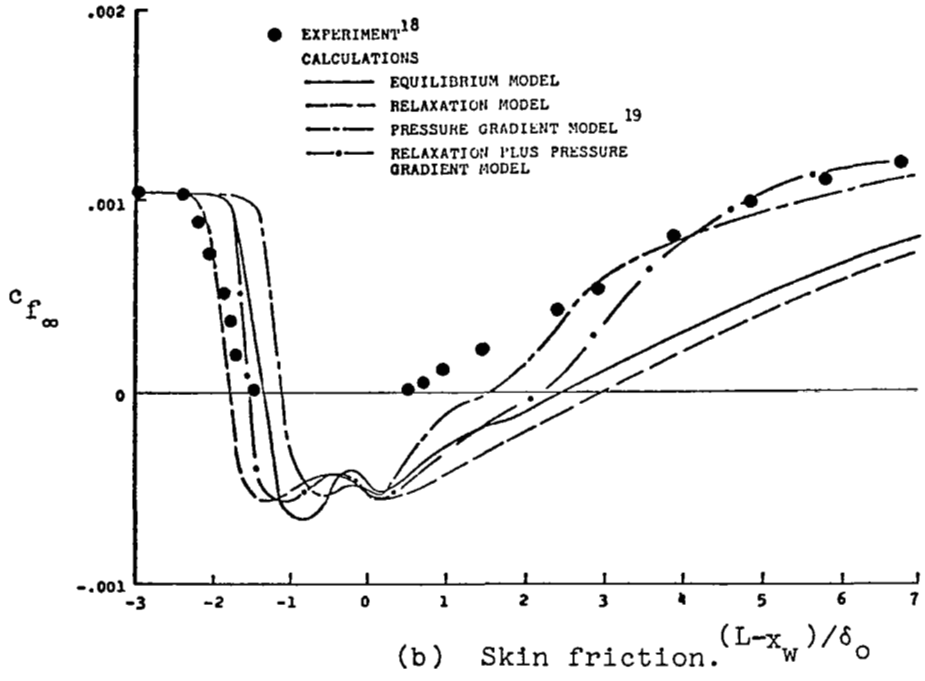

(b) Skin friction.

Figure 12. Comparison of computed and measured surface pressure and skin friction for the various relaxation models; $M_\infty = 2.85$, $\delta_o = .83$ in, $\alpha = 24°$, $Re_{\delta_o} = 1.3 \cdot 10^6$.

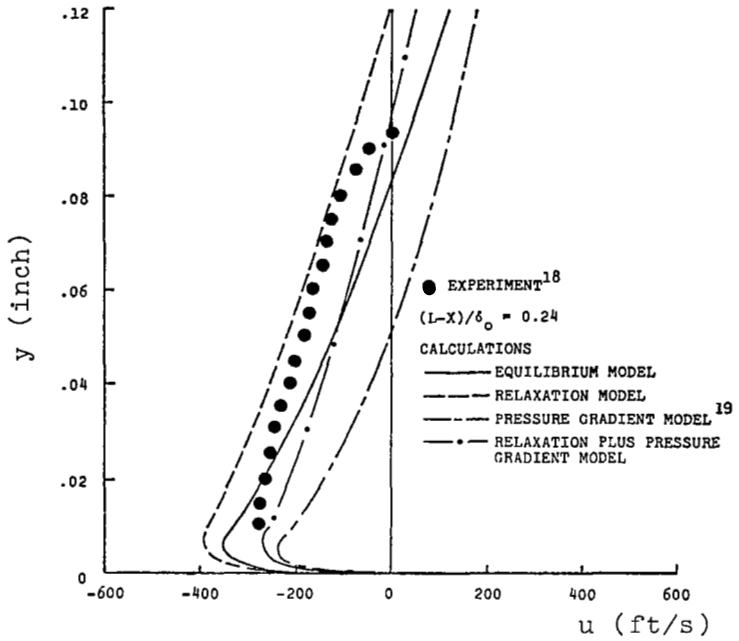

(a) Inside separation bubble.

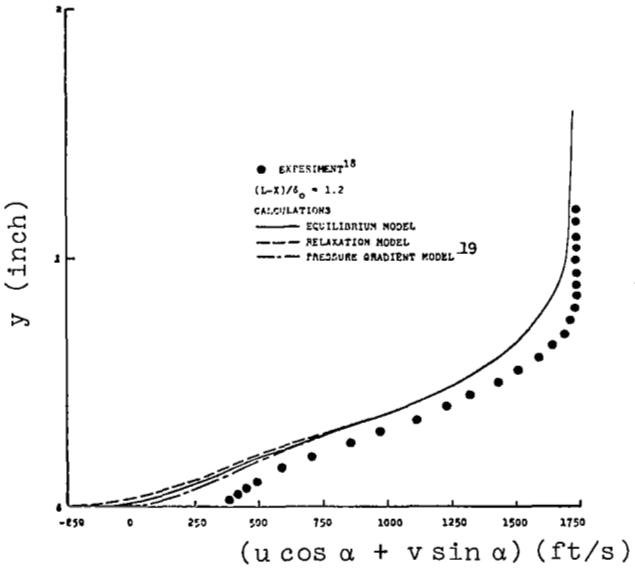

(b) Near reattachment.

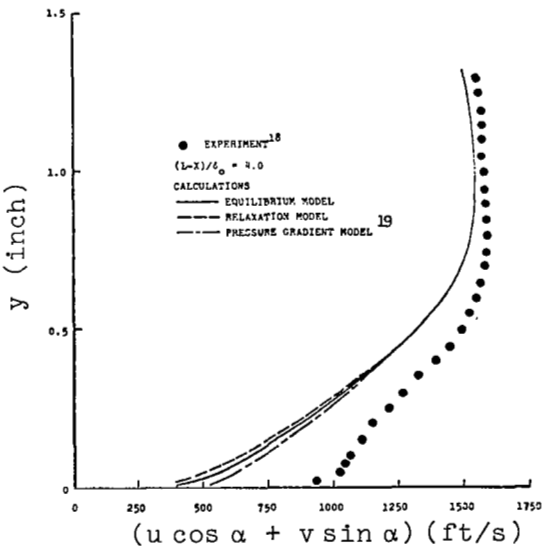

(c) Far downstream.

Figure 13. Comparison of computed and measured mean velocity field.

pressure gradient corrections do a good job of predicting skin friction far downstream of reattachment, the reattachment location itself is still incorrectly computed although in better agreement with experiment than for the equilibrium model. Additional comparisons with velocity profiles at three locations are shown in Figures 13(a)-13(c). As shown, in the bubble [Figure 13(a)] the experimental data are reasonably well predicted by the equilibrium and relaxation models, while the model employing only the pressure gradient correction underpredicts the bubble height. Far downstream at $(x_w-L)/\delta_o = 4$ [Figure 13(c)], all of the turbulence models give essentially the same results – all in substantial disagreement with experiment.

3.6 HYPERSONIC FLOW APPLICATIONS

At hypersonic speeds, compressibility makes drastic changes in the nature of turbulent flow. The turbulence disturbances are mostly composed of density and temperature fluctuations. At high hypersonic speeds, a slight local velocity change in the fluid would cause a large change in its temperature. Therefore, one might expect the test of turbulence model accuracy to be more severe in this case. Recall that the simple equilibrium eddy-viscosity model was originally derived based on the turbulent velocity fluctuations of incompressible flow. The purpose of this section is to investigate how the simple eddy viscosity model with relaxation behaves at high Mach numbers with heat transfer.

The experiments selected for comparison were conducted by Holden[20] and measurements were made of pressure, skin friction, and heat transfer along the wall. The flow conditions are as follows:

$M_\infty = 8.66$ $\quad Re_L = 2.2 \cdot 10^7$ $\quad T_w = 537°R$

$T_\infty = 119.5°R$ $\quad L = 2.25$ ft $\quad \alpha = 27°$ and $36°$

The wall is assumed to be isothermal and highly cooled; the ratio of wall temperature to adiabatic temperature is about $T_w/T_{aw} = 0.28$. As in the previous supersonic problem, a mesh with 63 points in the x-direction and 31 in the y-direction is used. Now, however, the fine mesh contains 21 points for better resolution. The upstream boundary is located at $x/L = 0.881$ with 23 points of equal space resolution between the upstream boundary and the hinge line of the wedge, which is $x/L = 1.0$. The mesh cells near the wall are very elongated with $\Delta x/(\Delta y)_{min} = 226$. The computation is advanced about 95 times in the inner mesh loop for every outer mesh timestep.

Figures 14 and 15 show the detailed comparisons of the present calculated results with the experimental measurements of surface pressure, heat transfer, and skin friction for $\alpha = 27°$ and 36°. The agreement is very good upstream of the interaction region. This implies that, at least in this study, the equilibrium eddy viscosity model can be used to predict equilibrium hypersonic turbulent flow over a flat plate. The fluctuations of temperature and density may be considered as a simple function of the fluctuation of velocity, and the simple eddy-viscosity relation does provide proper turbulence mixing in the equilibrium hypersonic, turbulent boundary layer.

Surprisingly enough, the results also show reasonably good agreement in surface pressure and heat transfer in the interaction region, although the peak heat transfer at the reattachment point is underpredicted. The present heat transfer results are significantly different from that of the laminar flow case studied.[14] Instead of very low heat transfer in the separation region as in the laminar case, the heat transfer, here, drops sharply near the separation point, rises rapidly to a value greater than its upstream condition, gradually increases in the pressure plateau region, and then sharply

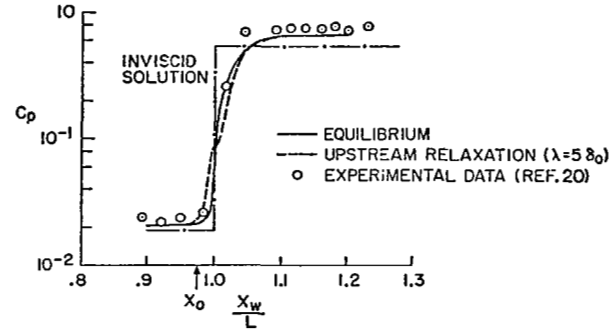

(a) Pressure coefficient.

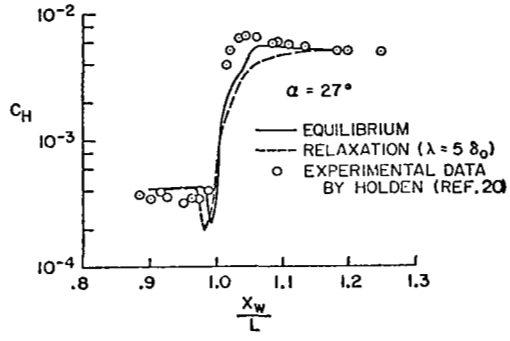

(b) Heat transfer.

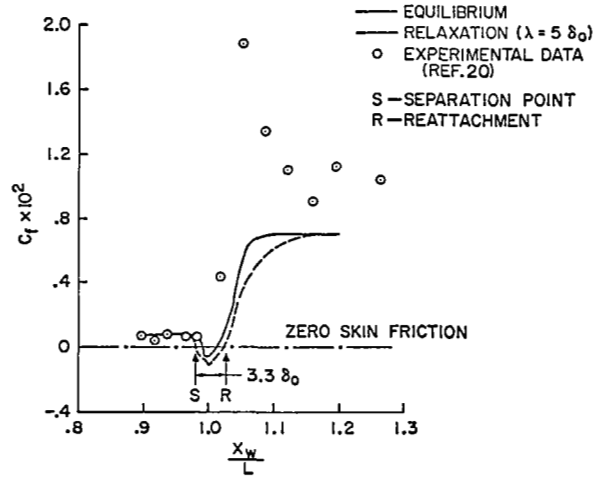

(c) Skin friction coefficient.

Figure 14. Comparisons of the results of equilibrium and relaxation models with experiments for $M_\infty = 8.66$, $\alpha = 27°$, $Re_L = 2.2 \cdot 10^7$, $L = 2.25$ ft, $\delta_o = 0.0323$ ft, $x_o/L = 0.9762$.

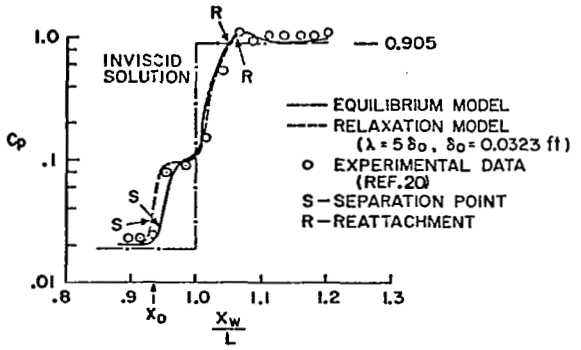

(a) Wall pressure.

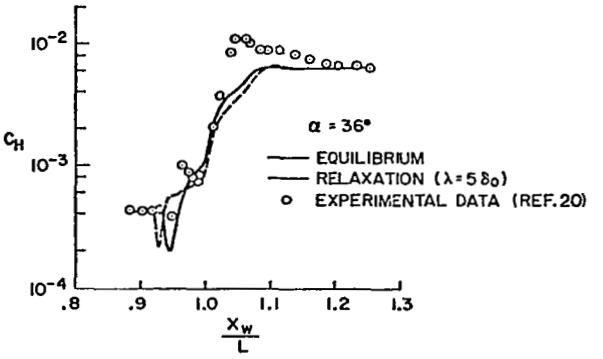

(b) Heat transfer coefficient.

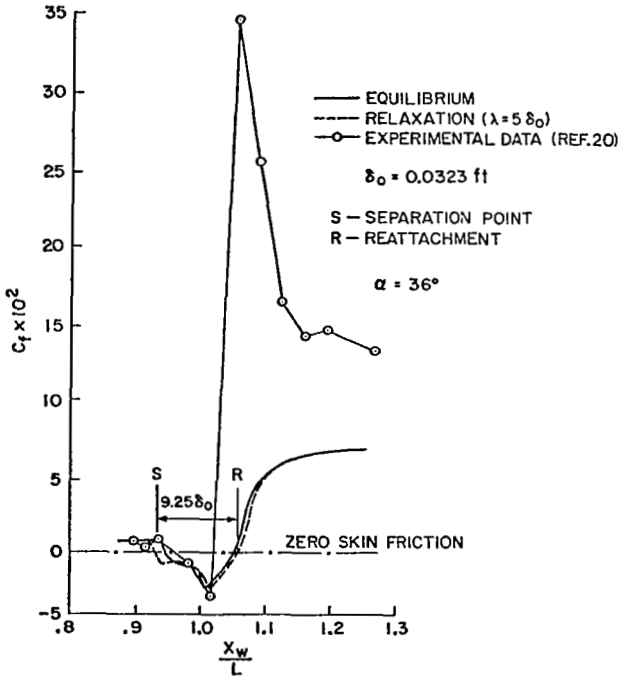

(c) Skin friction.

Figure 15. Comparisons of the results of equilibrium and relaxation models with experiments; $M_\infty = 8.66$; $\alpha = 36°$, $Re_L = 2.2 \cdot 10^7$, $T_W = 537°R$, $L = 27$ in, $x_o/L = 0.9392$.

increases under strong compression. As the separation region becomes larger, a heat transfer plateau region forms, similar to that of the surface pressure. In the experimental measurements, heat transfer does not show a sharp decrease at separation, and, instead of the slow gradual increase, it, indeed, shows a slight decrease in the pressure plateau region. It is still not clear whether the sharp, deep drop of heat trasnfer near the separation point is physically correct or is caused by the shortcomings of the simply eddy-viscosity model. As pointed out in the supersonic case (Figure 7), the eddy viscosity model tends to provide a very low value of eddy viscosity near the wall at the separation point. The underprediction of peak heat transfer in the reattachment region might also be caused by the same shortcoming of the turbulence model.

Unfortunately, even though the points of separation and reattachment are predicted with reasonable accuracy, the skin friction is grossly underpredicted in the regions of reattachment and downstream recompression. This strongly suggests that perhaps the value of eddy viscosity for the present hypersonic case is underpredicted in these highly compressed regions. From the experience of the previous frozen case result, it may be suspected that the predicted eddy viscosity is much less than the real value.

The application of the upstream relaxation process, also shown in Figures 14 and 15, does show increasing upstream pressure propagation. However, it also shows unfavorable effects of decreasing skin friction and heat transfer after reattachment, especially in the results of the $\alpha = 27°$ case, in which the separation region is small and the initial location x_o is positioned very close to reattachment. This may confirm our previous argument that the simple equilibrium eddy-viscosity model underpredicts the eddy viscosity value in the reattachment and

downstream recompression regions, and, moreover, the relaxation process reduces the eddy-viscosity value still further.

One interesting aspect of the strong compression associated with the hypersonic problem is the severe restriction imposed on $(\Delta y)_{min}$ along the wall. As shown in Figures 14(a) and 14(b), the pressure rises by a factor of about 30 for the case of $\alpha = 27°$ and about 50 for $\alpha = 36°$. The thickness of the boundary layer after compression is one order of magnitude thinner than that before the interaction. To ensure enough mesh resolution in the downstream highly compressed region, $(\Delta y)_{min}$ for the first mesh cell has to be very small. Figure 16 shows a plot of y^+ at the first mesh point versus x. At the upstream region, y_1^+ is far inside the sublayer ($y_1^+ \approx 0.52$), stays small in the separation region, and sharply increases right after the reattachment up to about 7. One should bear in mind that the present y_1^+ is evaluated based on the computed skin friction. For instance, if these values are calculated with the experimental skin friction, y_1^+ would increase by a factor of

$$\left[\tau_w(\text{experiment})/\tau_w(\text{calculated})\right]^{1/2} \approx (2)^{1/2}$$

for $\alpha = 27°$, which may result in a $y_1^+ \approx 10$ in the downstream region. However, y_1^+ is small in the separation region and the boundary layer in the downstream region is parabolic; hence, a y_1^+ of about 10 in the downstream region should primarily underpredict only the local skin friction and would not be expected to introduce significant error in the separation region.

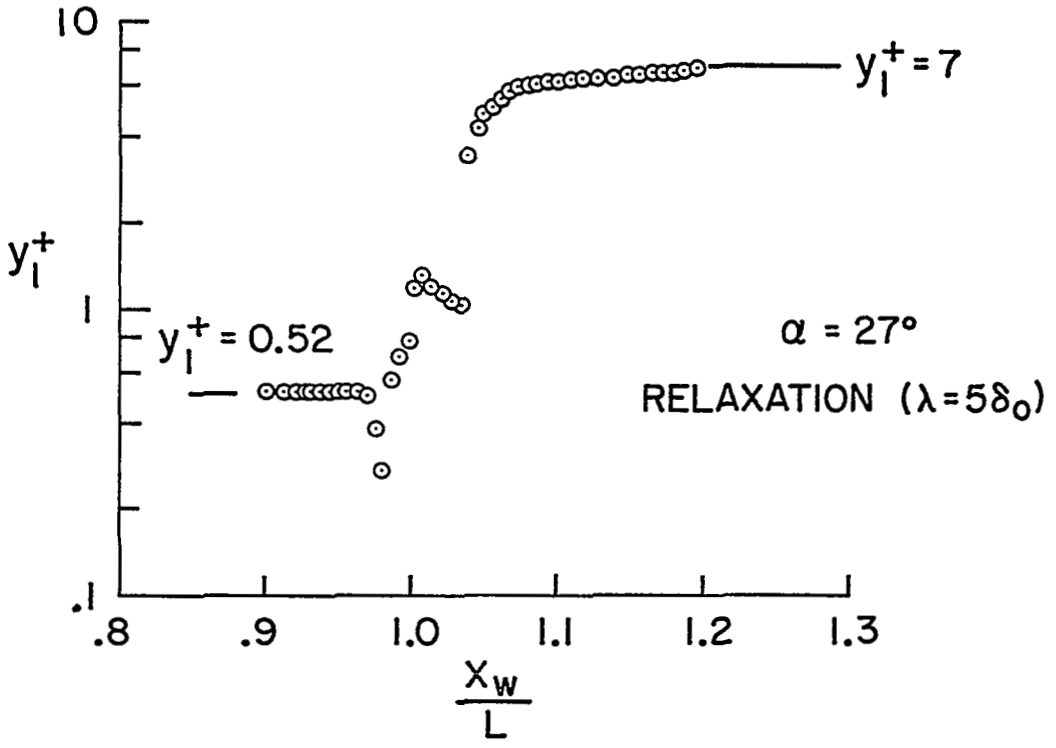

Figure 16. y^+ of the first mesh points along the x-direction for $\alpha = 27°$ (relaxation model.

4. SUMMARY AND CONCLUSIONS

Relaxation turbulence models have been intensively investigated. The complete time-dependent mass-averaged Navier-Stokes equations have been solved for flows over a two-dimensional compression corner. Computed supersonic solutions have been compared with the experimental measurements of Law and of Settles, Vas and Bogdonoff; also the hypersonic flows experimentally investigated by Holden have been numerically simulated. Details of the relaxation process have been studied; several different relaxation models, including different relaxation processes and varying relaxation length, have been tested and compared.

In general, the equilibrium model predicts a sharp increase of the outer layer eddy viscosity value near the separation shock, while the relaxation process substantially decreases the eddy viscosity and more accurately predicts upstream pressure propagation. The simple eddy-viscosity model predictions are in close agreement with measured upstream flow conditions in the hypersonic boundary layer. However, the model underpredicts the eddy viscosity, and hence, the skin friction in the reattachment and downstream recompression regions. Application of the relaxation process reduces the eddy-viscosity further, and shows unfavorable effects on heat transfer, skin friction, and reattachment point in these regions.

Finally, the relaxation process provides a simple technique for including upstream turbulence history and for controlling the magnitude of the eddy viscosity for flows subjected to strong and abrupt disturbances such as a shock wave. Results indicate that the eddy viscosity should be modified in the reattachment recompression region for both the inner and the outer layers;

the appropriate modification will yield substantially higher eddy viscosity values than those obtained with the equilibrium model.

REFERENCES

1. Bradshaw, P., "The Understanding and Prediction of Turbulent Flow," Aeronautical J 76, p 403 (July 1972).

2. Reynolds, W.C., "Computation of Turbulent Flows," Stanford University Report No TF-4 (April 1975).

3. Baldwin, B.S. and MacCormack, R.W., "Interaction of Strong Shock Wave with Turbulent Boundary Layer," AIAA Paper 74-558, Palo Alto, California (June 1974).

4. Jacobs, W., "Umformung eines turbulenten Geschwindigkeits-profiles," Z Angew Math Mech, Vol 19, pp 87-100 (1939).

5. Prandtl, L., "On a New Representation of Fully Developed Turbulence," JPL Publication No 13, A Translation by D. Coles (August 1952).

6. Rotta, J.C., "Turbulent Boundary Layers in Incompressible Flow," Progress in Aerospace Sciences, Vol 2, p 1 (1962).

7. Shang, J.S. and Hankey, W.L., "Numerical Solution of the Navier-Stokes Equations for Compression Ramp," AIAA Paper 75-4, Pasadena, California (January 1975).

8. Baldwin, B.S. and Rose, W.C., "Calculation of Shock-Separated Turbulent Boundary Layers," NASA-SP-347 (March 1975).

9. Shang, J.S., Hankey, W.L. and Law, C.H., "Numerical Simulation of Shock Wave-Turbulent Boundary-Layer Interaction," AIAA Paper 76-95, Washington, DC (January 1976).

10. Deiwert, G.S., "Computation of Separated Transonic Turbulent Flows," AIAA Paper 75-829, Hartford, Conn (June 1975).

11. Mateer, G.G., Brosh, A. and Viegas, J.R., "A Normal Shock-Wave Turbulent Boundary-Layer Interaction at Transonic Speeds," AIAA Paper 76-161, Washington, DC (January 1976).

12. Marvin, J.G. and Sheaffer, Y.S., "A Method for Solving the Nonsimilar Laminar Boundary-Layer Equations Including Foreign Gas Injection," TN D-5516, NASA.

13. MacCormack, R.W. and Baldwin, B.S., "A Numerical Method for Solving the Navier-Stokes Equations with Application to Shock-Boundary Layer Interactions," AIAA Paper 75-1, Pasadena, Calif (January 1975).

14. Hung, C.M. and MacCormack, R.W., "Numerical Solutions of Supersonic and Hypersonic Laminar Flows over a Two-Dimensional Compression Corner," AIAA Paper 75-2, Pasadena, Calif (January 1975).

15. MacCormack, R.W., "An Efficient Numerical Method for Solving the Time-Dependent Compressible Navier-Stokes Equations at High Reynolds Number," NASA TMX-73129 (July 1976).

16. Law, C.H., "Supersonic Turbulent Boundary Layer Separation," AIAA J 12, No 6, p 794 (June 1974).

17. Havener, A.G. and Radley, R.J., "Supersonic Wind Tunnel Investigations Using Pulsed Laser Holography," ARL 73-0148, Aerospace Research Laboratories, Wright-Patterson AFB, Ohio (October 1973).

18. Settles, G.S., Vas, V.E., and Bogdonoff, S.M., "Shock Wave-Turbulent Boundary Layer Interaction at a High Reynolds Number, Including Separation and Flow Field Measurements," AIAA Paper 76-164, Washington, DC (January 1976).

19. Horstman, C.C., "A Turbulence Model for Nonequilibrium Adverse Pressure Gradient Flows," AIAA Paper 76-412, San Diego, Calif (July 1976).

20. Holden, M.S., "Shock Wave-Turbulent Boundary Layer Interaction in Hypersonic Flow," AIAA Paper 72-74, San Diego, Calif (Supplemental data included in private communication) (January 1972).